

****FULL TITLE****

*ASP Conference Series, Vol. **VOLUME**, **YEAR OF PUBLICATION***

****NAMES OF EDITORS****

Simulations of the Magneto-rotational Instability in Core-Collapse Supernovae

M. Obergaulinger, P. Cerdá-Durán, and E. Müller

Max-Planck-Institut für Astrophysik, Postfach 1317, D-85741 Garching, Germany

M.A. Aloy

Departament d'Astronomia i Astrofísica, Universitat de València, Edifici d'Investigació Jeroni Muñoz, C/ Dr. Moliner, 50, E-46100 Burjassot (València), Spain

Abstract. We assess the importance of the magneto-rotational instability in core-collapse supernovae by an analysis of the growth rates of unstable modes in typical post-collapse systems and by numerical simulations of simplified models. The interplay of differential rotation and thermal stratification defines different instability regimes which we confirm in our simulations. We investigate the termination of the growth of the MRI by parasitic instabilities, establish scaling laws characterising the termination amplitude, and study the long-term evolution of the saturated turbulent state.

1. Introduction

At the end of its hydrostatic evolution, the inner core of a star of more than about eight solar masses, consisting of about 1.5 solar masses of iron or oxygen, neon, and magnesium loses support against its self-gravity and collapses to supranuclear density $\rho_{\text{nuc}} \geq 2 \times 10^{14} \text{ g cm}^{-3}$, releasing a gravitational binding energy $E_{\text{grv}} \sim 10^{53} \text{ erg}$. When this density is reached, a shock wave is launched and starts to propagate outward. Still within the core, the shock wave stalls and turns into a stationary accretion shock as energy is lost when nuclei are dissociated in the post-shock region: the prompt explosion fails.

Most of the gravitational binding energy liberated during collapse leaves the star in form of neutrinos, but a small ($\sim 1\%$) fraction is used to unbind the envelope and power a supernova (SN) explosion. How a fraction of E_{grv} is transferred to the shock wave and the surrounding envelope is still not fully understood, and forms the central issue of SN theory.

This is not a problem of energy budget but of energy transfer. The gravitational binding energy of the envelope ($\sim 10^{50} \text{ erg}$) as well as the kinetic and electromagnetic energies of a SN ($\sim 10^{49}$ and $\sim 10^{51} \text{ erg}$, respectively) are much smaller than E_{grv} . Consequently, the transfer of a small fraction of E_{grv} suffices to revive the shock wave and to trigger the explosion. However, it is extremely difficult to tap efficiently the energy carried by weakly interacting neutrinos. The mechanisms proposed to account for shock revival and explosion can be grouped into the following categories:

The spherical neutrino mechanism Heating of the post-shock matter by interactions with the neutrinos diffusing out of the core revives the shock (e.g., Bethe 1990). This mechanism works for stars around $8 M_{\odot}$ due to a steep density profile facilitating shock propagation (Kitaura et al. 2006).

Hydrodynamic instabilities Without the restriction to spherical symmetry, hydrodynamic instabilities can develop: convection in the proto-neutron star (PNS) and behind the shock and the standing accretion shock instability (SASI) can enhance the efficiency of neutrino heating and the transfer of binding energy of the accreting gas to the surrounding matter (Blondin et al. 2003; Foglizzo et al. 2007). They may also account for the pronounced asphericities of the explosion and the observed pulsar kicks (e.g., Scheck et al. 2006). While this mechanism has proven successful in detailed 2d simulations of stars up to 15 solar masses employing state-of-the-art microphysics (Marek et al. 2009), its robustness and applicability to stars of higher mass is still uncertain.

Energy transfer by waves Apart from neutrinos, waves may carry energy from the central region to the surroundings. Unstable g-modes in the PNS excited by accreting matter can lead to the emission of acoustic waves travelling upwards and depositing energy near the shock (Burrows et al. 2006). A similar effect can be caused by Alfvén waves excited in the convective region of a magnetised PNS (Suzuki et al. 2008). The importance of acoustic waves has been suggested in simulations, whereas the heating by Alfvén waves has not been explored thoroughly.

Rotational mechanisms Any rotation of the progenitor will be amplified during the collapse; additionally, differential rotation will be created even for an initially rigidly rotating progenitor. If sufficiently rapid, rotation may provide sufficient additional energy to unbind the post-shock matter. In contrast to the energy of neutrinos, rotational energy can be tapped fairly easily, e.g., by viscosity or magnetic fields (Thompson et al. 2005). Additionally, a differentially rotating magnetised fluid can be unstable against the magneto-rotational instability (MRI) (Balbus & Hawley 1991, 1998), leading to field amplification, turbulence and enhanced transport of angular momentum.

None of these mechanisms has been able to provide a robust explanation for SNe across the entire mass range. Because of the diversity and complexity of the underlying physics, the problem is studied using complementary approaches: very detailed simulations including the best treatment of the microphysics that can be afforded and, on the other hand, simplified models neglecting most of these complications for the benefit of covering a larger parameter space of initial conditions. The study of (magneto-)rotational mechanism relies currently mostly on simplified models.

Akiyama et al. (2003) have pointed out that the most basic instability condition of the MRI, i.e., a negative radial gradient of the rotational profile, $\Omega(r)$, is typically fulfilled in rotating post-collapse cores. They have, based on simplified spherical modelling, estimated growth times of a few milliseconds and saturation fields of the order of 10^{15} G. Simplified global simulations (e.g.,

Obergaulinger et al. 2006) have shown that fields of this range (reached only for already strongly magnetised progenitors with fields of the order 10^{12} G) can have significant effects on the dynamics of the explosion, e.g., by extracting rotational energy from the inner core or launching jet-like outflows. Additionally, signs for the growth of the MRI were found in a few of those simulations. Based only on such simplified studies, a thorough assessment of the influence of the MRI is still not possible.

2. Methods and Aim of our Study

The main obstacle for investigating the MRI by detailed microphysical simulations is the necessity to resolve the wavelength of the most unstable MRI modes, λ_{MRI} , which scales with the local Alfvén velocity, leading to a prohibitive resolution requirement: for a realistic initial field of 10^9 G, a region of several 100 kilometres would have to be covered by a 3d grid with a resolution of a few centimetres or metres. Consequently, we investigated the properties of the MRI in core-collapse SNe using high-resolution simulations of small representative domains in the unstable region (Obergaulinger et al. 2009).

We studied basic properties of the MRI in the linear regime under typical conditions of post-collapse cores differing from the well-studied case of accretion discs mainly by the spherical geometry and the potential importance of thermal stratification exerting either a stabilising or a destabilising effect on the MRI. Since the absolute value of the Brunt-Väisälä frequency, N , of the star can exceed Ω strongly, the dynamics of the core may not be dominated by standard MRI modes but rather show a more complex interplay between the MRI and hydromagnetic convection.

Even if the instability grows fast enough, it can affect the explosion only if a sufficiently large mean total (Maxwell plus Reynolds) stress tensor is reached at the termination of the growth and maintained during the turbulent saturated phase. This is a long-standing issue in MRI theory, and no final solution has been found although simulations have identified a number of factors, physical and numerical, affecting the amplitudes. We tried to estimate the saturation amplitude by an analysis of the non-linear phase of our models.

3. Results

3.1. Instability Analysis

We analysed the dispersion relation of wave-like perturbations of a background in rotational equilibrium endowed with a weak magnetic field with given rotational profile and Brunt-Väisälä frequency, N , i.e., the oscillation frequency of a buoyant fluid element (which is imaginary in a convectively unstable layer). Different from accretion discs, the main stabilising agent counteracting gravity is not rotation but pressure. Thus, the corresponding models possess a sub-Keplerian rotation.

The instability criteria, given by Balbus (1995), allow for two branches of unstable modes: *buoyant* and *Alfvén* modes, corresponding to unstable buoyant

oscillations and unstable Alfvén waves, respectively. Both branches are stabilised by magnetic tension at very short wavelengths.

Apart from a stable region of strongly positive gradients of entropy or Ω , these modes dominate in two different regions of the parameter space. For a negative entropy gradient and moderate (positive or negative) values of N^2 , corresponding to a small influence of the thermal stratification, Alfvén modes dominate. They grow most rapidly in a narrow wavelength region around λ_{MRI} and have a vanishing growth rate at infinite wavelength, leading to stringent resolution requirements in numerical simulations. If $-N^2 > 0$ exceeds a threshold, buoyant modes set in, while Alfvén modes disappear. Similar to convection in a non-magnetised fluid, they grow rapidly from infinite to short wavelengths.

Based on the relative importance of these modes, we can distinguish six regions in the space given by the Brunt-Väisälä frequency and the rotational profile: a stable region, the classic (accretion-disc) MRI, Rayleigh instability, magnetoconvection, a region in which the stabilisation of convection due to rapid (rigid) rotation is lifted by magnetic fields, and a mixed regime, respectively.

3.2. Numerical Models

We performed a large parameter study of simplified 2d and 3d simulations representing small (a few kilometres wide) sections of the equatorial region of a post-collapse core with a cylindrical mesh of a resolution between 0.625 and 20 metres. We added a weak magnetic field in vertical, z , direction, either uniform or sinusoidally varying with a vanishing net flux, to the gas assumed in rotational equilibrium with a prescribed rotational profile and entropy gradient.

To save computational costs, we neglected neutrino transport entirely and replaced the complex nuclear equation of state by a simple analytic approximation. Our numerical code is based on a conservative formulation of the equations of ideal MHD within the constrained-transport framework (Evans & Hawley 1988) and uses high-order methods for reconstruction (e.g., the monotonicity-preserving schemes by Suresh & Huynh 1997) and approximate Riemann solvers.

The simulations confirm all regimes relevant to the MRI in SNe, with numerical growth rates very well in agreement with the analytic predictions. Under conditions of a rapidly rotating core, we expect typical MRI growth times of the order of a few milliseconds, i.e., sufficiently fast to affect the explosion developing on time scales of several tens or hundreds of milliseconds (see the left panel of Fig. 3.2. for the time evolution of a model with vanishing net flux).

The initial perturbations grow exponentially at the MRI growth rate given by linear analysis, σ_{MRI} . Their growth is mediated by coherent large-scale *channel modes*, i.e., axisymmetric pairs of upflows and downflows with alternating magnetic polarity. As shown by Goodman & Xu (1994), the channel modes are themselves unstable against secondary, *parasitic* instabilities of Kelvin-Helmholtz or tearing-mode type. Our models show the growth of these parasites feeding off the channel modes. Their growth rate is a function of the field strength of the channels. The higher the field strength of a channel is, the faster grow its parasites, until, at a certain field strength, the amplitude of the parasites exceeds that of the channel: the MRI growth terminates. In the left panel of Fig. 3.2., the growth of these parasites can be identified by the strong increase of the z -component of the magnetic field near $t = 12$ ms. Typically, the para-

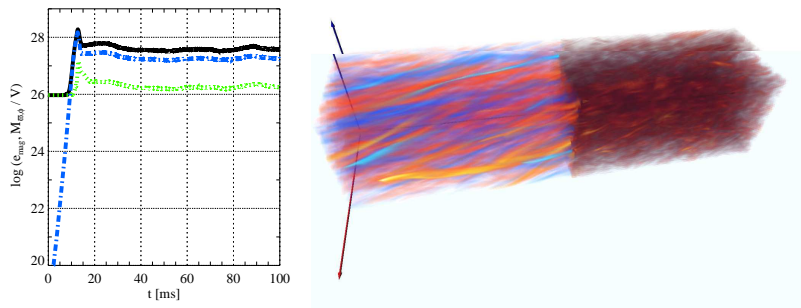


Figure 1. The time evolution of a model with vanishing net flux of the magnetic field (left panel) and its spatial structure in the saturated state (right panel). The left panel shows the total magnetic energy (black solid line), its z -component (green dotted line), and the Maxwell stress component $M_{\varpi\phi} = b_{\varpi}b_{\phi}$ (blue dash-dotted line) per unit volume as a function of time in milliseconds. The right panel shows the computational box; the radial, azimuthal, and vertical directions are indicated by the red (pointing towards the observer), green (hidden, pointing to the right), and blue (pointing up) arrows. The left and right halves of the figure show a volume rendering of the toroidal magnetic field, b_{ϕ} , (positive and negative values are shown by blue and red colours) and of the vorticity of the flow, respectively.

sitic mode quenching the MRI in our models is of tearing-mode type. This is clearly an artefact of our numerics. Since we evolve the system of *ideal* MHD there should be no resistivity, and thus no tearing-mode instability. However, the unavoidable numerical resistivity, albeit only at a small level, permits the growth of resistive instabilities.

Combining the MRI growth rates from linear analysis and those of the parasites determined in a series of auxiliary simulations, we establish scaling laws for the value of the Maxwell stress at the termination of MRI growth. A stronger initial field, b_0 , corresponds to wider channel flows which can sustain a stronger field before they are disrupted by parasites. Consequently, the termination amplitude scales with the initial field as $(b_0)^{16/7}$. A higher grid resolution, δ , corresponds to a smaller value of the numerical resistivity, and thus to a slower growth of the parasites, leading to a scaling of the termination amplitude as $\delta^{-8/7}$. Slower rotation leads to wider channels, again decreasing the growth of parasites. Hence we find a scaling with $\Omega^{8/7}$. Finally, the growth rate of the parasites depends on the local sound speed, yielding a scaling with $c_s^{6/7}$.

After the disruption of the coherent channel flows, turbulence develops (see Fig. 3.2., right panel, for the structure of a model in this state). The flow and the magnetic field (shown in the right and left halves of the panel) are characterised by a multitude of small-scale filamentary features. Most obvious are magnetic flux tubes elongated in azimuthal direction. Depending on the MRI regime and the predominance of Alfvén (buoyant) modes, efficient transport of angular momentum (entropy) leads to rigid rotation (flat entropy profile, and a rotation profile where the specific angular momentum is constant).

The Maxwell stress is typically maintained at a level of the order of its termination value throughout saturation, but it is subject to pronounced oscil-

lations and even intermittent episodes of exponential growth. These correspond to the re-appearance of coherent channel-like flows that terminate after a short time by parasitic modes (Sano & Inutsuka 2001). Apart from these flows, we identify large-scale correlations of the velocity and magnetic field in the turbulence maintained over several orbital periods, similar to the ones observed by Lesur & Ogilvie (2008).

Our results suggest that the MRI may play a role, for SNe that have rapidly rotating progenitors. The field strengths reached in our models are of the order of 10^{15} G, i.e., sufficiently strong to affect the explosion by redistributing angular momentum and extracting energy from rotation. For slower rotation, the interplay of the MRI and convection, i.e., the mixed instability regime may play a role in the unstable regions of the PNS and the surrounding neutrino-heated hot bubble. Neglecting a large part of the relevant physics and restricting ourselves to a rather special geometry, we are, however, far from a final answer, e.g., in the form of a MRI model with predictive power for generic post-collapse cores. Further modelling is required to include the effects neglected thus far.

Acknowledgments. This research has been supported by the Spanish *Ministerio de Educación y Ciencia* (grants AYA2007-67626-C03-01, CSD2007-00050), and by the Collaborative Research Center on *Gravitational Wave Astronomy* of the Deutsche Forschungsgemeinschaft (DFG SFB/Transregio 7). MAA is a Ramón y Cajal fellow of the *Ministerio de Educación y Ciencia*. Most of the simulations were performed at the Rechenzentrum Garching (RZG) of the Max-Planck-Society. We are also thankful for the computer resources, the technical expertise, and the assistance provided by the Barcelona Supercomputing Center - Centro Nacional de Supercomputación. Finally, we would like to A. Marek for helpful discussions.

References

- Akiyama, S., Wheeler, J. C., Meier, D. L., & Lichtenstadt, I. 2003, ApJ, 584, 954
 Balbus, S. A. 1995, ApJ, 453, 380
 Balbus, S. A. & Hawley, J. F. 1991, ApJ, 376, 214
 Balbus, S. A. & Hawley, J. F. 1998, Reviews of Modern Physics, 70, 1
 Bethe, H. A. 1990, Reviews of Modern Physics, 62, 801
 Blondin, J. M., Mezzacappa, A., & DeMarino, C. 2003, ApJ, 584, 971
 Burrows, A., Livne, E., Dessart, L., Ott, C. D., & Murphy, J. 2006, ApJ, 640, 878
 Evans, C. R. & Hawley, J. F. 1988, ApJ, 332, 659
 Foglizzo, T., Galletti, P., Scheck, L., & Janka, H.-T. 2007, ApJ, 654, 1006
 Goodman, J. & Xu, G. 1994, ApJ, 432, 213
 Kitaura, F. S., Janka, H.-T., & Hillebrandt, W. 2006, A&A, 450, 345
 Lesur, G. & Ogilvie, G. I. 2008, A&A, 488, 451
 Marek, A., Janka, H.-T., & Müller, E. 2009, A&A, 496, 475
 Obergaullinger, M., Aloy, M. A., & Müller, E. 2006, A&A, 450, 1107
 Obergaullinger, M., Cerdá-Durán, P., Müller, E., & Aloy, M. A. 2009, A&A, 498, 241
 Sano, T. & Inutsuka, S.-i. 2001, ApJ, 561, L179
 Scheck, L., Kifonidis, K., Janka, H.-T., & Müller, E. 2006, A&A, 457, 963
 Suresh, A. & Huynh, H. 1997, J. Comput. Phys., 136, 83
 Suzuki, T. K., Sumiyoshi, K., & Yamada, S. 2008, ApJ, 678, 1200
 Thompson, T. A., Quataert, E., & Burrows, A. 2005, ApJ, 620, 861